Journal of the Serbian Chemical Society
JSCS-info@shd.org.rs • www.shd.org.rs/JSCS
J. Serb. Chem. Soc. *88* (1) 41–54 (2023)
JSCS–5609
Original scientific paper
Published 23 November 2022

Electrochemical properties of carbonized bentonite

NATAŠA P. JOVIĆ-JOVIČIĆ[1], DANICA V. BAJUK BOGDANOVIĆ[2#], TATJANA B. NOVAKOVIĆ[1], PREDRAG T. BANKOVIĆ[1], ALEKSANDRA D. MILUTINOVIĆ-NIKOLIĆ[1#] and ZORICA D. MOJOVIĆ[1]*

[1]*University of Belgrade – Institute of Chemistry, Technology and Metallurgy, Department of Catalysis and Chemical Engineering, Njegoševa 12, 11000 Belgrade, Serbia and* [2]*Faculty of Physical Chemistry, University of Belgrade, Studentski Trg 12–16, 11000 Belgrade, Serbia*

(Received 27 January, revised 22 March, accepted 26 March 2022)

Abstract: Organomodified bentonites were obtained by modification of bentonite clay from local mine Bogovina, with four different alkylammonium ions in the amounts that correspond to cation exchange capacity. Carbonized bentonites, obtained by pyrolyzing the organomodified bentonites in the flow of nitrogen, were characterized using XRD, low-temperature N_2 physisorption and Raman spectroscopy. Structural and textural properties of carbonized bentonites depended on the arrangement of alkylammonium cations in the paternal organomodified bentonite, while the Raman spectroscopy confirmed the presence of amorphous carbon. The obtained carbonized bentonites were used for modification of the carbon paste electrode. The modified electrodes were investigated using cyclic voltammetry and electrochemical impedance spectroscopy. The electrosorption of chloride and sulfate anions on carbonized bentonites was studied by chronocoulometry. The results were interpreted in the terms of surface groups and textural properties of the carbonized bentonites.

Keywords: $Fe(CN)_6^{3-/4-}$; electrosorption; chlorides; sulfates.

INTRODUCTION

Clays are materials with a wide range of application, present in plentiful deposits on or near the surface of the Earth. The smectite type of clays, such as bentonite, is of particular interest. Because of the properties such as high cation exchange capacity, surface area, and hydration characteristics, smectites can easily undergo a vast variety of modifications.[1]

Clay-modified electrodes have been investigated for a couple of decades to alter the electrode surface, consequently facilitating the reactions that occur on that surface.[2–5] Differently treated clays were used for electrode modification.

* Corresponding author. E-mail: zorica.mojovic@ihtm.bg.ac.rs
# Serbian Chemical Society member.
https://doi.org/10.2298/JSC220127030J

The most used are acid activation,[6] pillaring[7] and modification by organic compounds.[8] Each of these modifications brought new properties to the composite material broadening the range of their applications (as electrochemical sensors for a variety of analytes,[9] electrodes for energy storage applications, ion-selective electrodes). Among these applications, the electrochemical sensors for pharmaceutical[10] and food quality[11] can be singled out as the most advanced ones.

Further improvement of clay electrodes has been attempted through the synthesis of carbon-clay composites.[12–14] The carbon-clay composites combined a relatively high specific surface area of the clay with a good electrical conductivity of carbon and can open new possible applications of these hybrid materials.

Carbon electrodes are used for capacitive deionization of water, among other applications. This area of investigation acquired great attention in the last years due to worldwide problems regarding the lack of clean freshwater.[15] This work aims to establish the potential usability of carbonized bentonites for capacitive deionization. In the previous publication of this group of authors[16] carbon-clay composites were obtained by carbonizing clays modified with different amounts of hexadecyltrimethylammonium (HDTMA) ion. The performance of carbonized samples and parenting organomodified samples was compared. The results showed that the amount of present organic precursor had a significant influence on the electrochemical properties of the resulting carbonized clay. It was concluded that the electroactivity of carbonized clay-based electrodes depended on the porosity, ion-exchange capacity, and carbon-clay interface contact. One of the important parameters for efficient electrosorption is the behaviour of the electrode/electrolyte interface. The pore size distribution, rather than specific surface area, is one of the main factors influencing the formation of an electric double layer, and therefore the efficiency of electrosorption.[17] In this work the influence of different organic precursors on the electrochemical properties of resulting carbonized bentonite was investigated. Bentonite clay from a local deposit (Bogovina, Serbia) was modified with four different alkylammonium anions. The response of the obtained carbonized bentonites was tested toward negatively charged redox probe as well as for the electrosorption of chloride and sulfate ions.

EXPERIMENTAL

Bentonite (clay from Bogovina, coal and bentonite mine, Serbia) fraction with a particle size of up to 74 μm, enriched with sodium using the ion-exchange procedure, was employed for modification with different organic cations. The procedure for organo-bentonite preparation was adopted according to Baskaralingam.[18] Four alkylammonium ions (hexadecyltrimethylammonium (HDTMA), dodecyltrimethylammonium (DDTMA), benzyltrimethylammonium (BTMA) and trimethylammonium (TMA), all acquired from Sigma–Aldrich) were introduced in the amounts which correspond to the value of cation exchange capacity (*CEC*) of the clay. The *CEC* value was previously estimated by ammonium acetate procedure (EPA, Method 9080)[19] to be 63.3 mmol of monovalent cation per 100 g of dry clay.[20] The obtained organomodified bentonites were heated at the rate of 5 °C min^{-1} until 400 °C was

reached. The temperature was held at 400 °C for 30 min. Subsequently, the samples were let to cool down to room temperature. The cycle of heating and cooling was performed in the stream of nitrogen. The samples were designated as c-HDTMA-B, c-DDTMA-B, c-BTMA-B and c-TMA-B, per the applied parental material.

The XRD analysis was performed using a Rigaku Smart Lab automatic multipurpose X-ray diffractometer (equipped with low background Si sample holder support; 1D D/teX 250 Ultra detector in XRF mode) and Cu anode (λ = 0.1542 nm). The diffractograms of the samples were obtained in the 2θ range from 2 to 45°, with the scanning rate of 0.3° min^{-1}, and scanning step of 0.01°.

Textural properties were assessed from nitrogen adsorption-desorption isotherms recorded at −196 °C and relative pressure in the range $0.05 < p/p_0 < 0.98$ using a Sorptomatic 1990, Thermo Finnigan. Samples were degassed at 150 °C for 10 h under vacuum. The specific surface area of the samples was calculated according to the Brunauer, Emmett and Teller (BET) method from the linear part of the nitrogen adsorption isotherms.[21–23] The pore size distribution has been computed from the desorption branch of the isotherms using Barrett, Joyner and Halenda (BJH) method.[21]

The Raman spectra were recorded using a Thermo DXR Raman microscope and laser excitation at the wavelength of 532 nm. Measurements were performed using the constant laser power of 9 mW, exposure time of 20 s, repetition of 10, grating with 900 lines mm^{-1}, and spectrograph aperture of 50 μm pinhole. The Thermo Scientific Omnic 9 software was used for the spectra acquisition and analysis. After the acquisition, the fluorescence background was subtracted from the Raman spectra using the fifth-order polynomial fit.

The electrochemical investigation of the samples was performed using modified a carbon paste electrode as the working electrode. Carbon pastes with the carbonized bentonite samples as modifiers were prepared manually by mixing 500 mg of a sample, 25 mg of carbon black (CB, Vulcan®-XC 72R), and 300 mg of paraffin oil. The paste was packed into a hollow (2 mm diameter) Teflon tube while the electrical contact was provided using a copper wire. The reference electrode was Ag/AgCl in 3 M KCl, while a platinum rod served as the counter electrode. The electrochemical measurements were performed using an Autolab electrochemical workstation (Autolab PGSTAT302N, Metrohm-Autolab BV, Netherlands). Impedance measurements were performed in 1 mM $K_4[Fe(CN)_6]$ in 0.2 M KCl, at open circuit potential using a 5 mV rms sinusoidal modulation in the 100 kHz–0.1 Hz frequency range. Cyclic voltammetry measurements were performed in the same electrolyte, at the scan rate of 50 mV s^{-1}. The electrosorption properties of carbonized clays were tested in 0.2 M NaCl and 0.2 M Na_2SO_4 solutions using chronocoulometry. Chronocoulometric curves were obtained by applying a potential of 0.5 V *vs*. Ag/AgCl for 20 s and recording the transient current.

RESULTS AND DISCUSSION

XRD analysis

The results of the XRD analysis for the carbonized samples are presented in Fig. 1.

The crystalline phases expected for bentonite were observed: smectite, quartz, feldspar and calcite.[24] It is well known that the incorporation of quaternary ammonium cations (QAC) into interlamellar space results in the increase of d_{001} values of smectite.[1] The previous studies of this group have shown that the incorporation of QAC in the different amounts corresponding to the cation exchange

capacity (*CEC*) of smectite leads to the formation of different molecular arrangements, depending on the structure and QAC alkyl chain length.[16,25–27] Short-chain QAC dominantly forms monolayers with characteristic $d_{001} \approx 1.4$ nm, while longer chain QAC make bilayers structure ($d_{001} \approx 1.8$ nm) with the alkyl chain axes parallel to the silicate layers.[1] Pseudo-trimolecular arrangement structures of kinked alkyl chains are observed with highly charged smectites and/or long surfactant cations and exhibit $d_{001} \approx 2.2$ nm.[1] The specific arrangements of organic cations in samples with the amount of QAC equal to *CEC* are summarized in Table I.

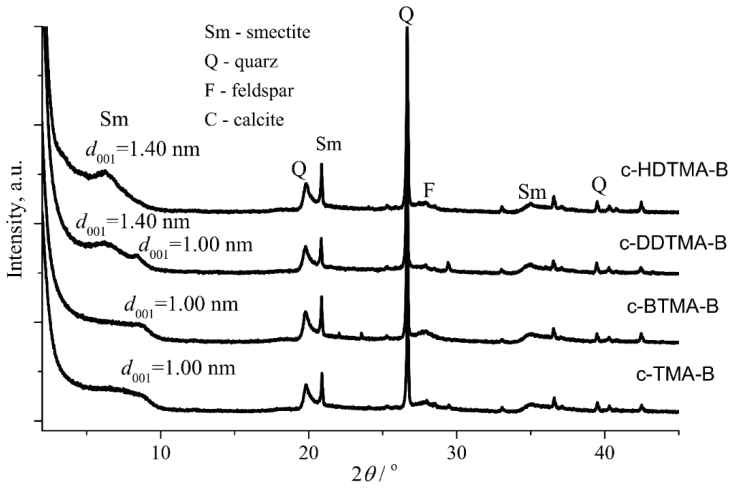

Fig. 1. X-ray diffractograms of carbonized bentonites (Sm – smectite, Q – quartz, F – feldspar and C – calcite).

TABLE I. Basal spacing values previously obtained for the samples with QAC incorporated in the amount equal to CEC

Sample	d_{001} / nm	QAC arrangement	Ref.
HDTMA-B	2.00	Pseudo-trimolecular layer	13
DDTMA-B	1.78	Bimolecular layer	22
BTMA-B	1.46	Monomolecular layer	23
TMA-B	1.40	Monomolecular layer	24

c-HDTMA-B, obtained by the carbonization of 1.0 HDTMA-B, showed $d_{001} = 1.40$ nm which is in agreement with the previous findings.[28] Taken into account that the elemental silicate sheet of Bogovina smectite is approx. 1.01 nm[28] the interlamellar distance of 0.40 nm is almost the same as reported by Ruiz-García *et al.*[29] for sucrose carbonated smectite.

The value of 0.40 nm is in good agreement with the formation of a carbon monolayer between smectite lamellae.[29,30] According to literature data, the type

of organic precursor and clay mineral had a strong impact on the formation of carbon structure and thickness.[29–31] The c-DDTMA-B besides the presence of d_{001} of 1.40 nm also showed the reflection that corresponded to collapsed structure with the characteristic basal spacing of ~1.0 nm.[1] Only the collapsed structure was detected for c-TMA-B and c-BTMA-B samples derived from the short--chain and the aromatic QAC precursors, respectively. Based on the obtained results, it seems that the samples with lower carbon content, either due to the smaller number of carbon atoms present in QAC precursor or lower loading of QAC,[16] led to the formation of the collapsed structure during the applied carbonization procedure at elevated temperature.

Textural properties

Nitrogen adsorption/desorption isotherms for carbonized bentonites (Fig. 2a) exhibited similar profiles.

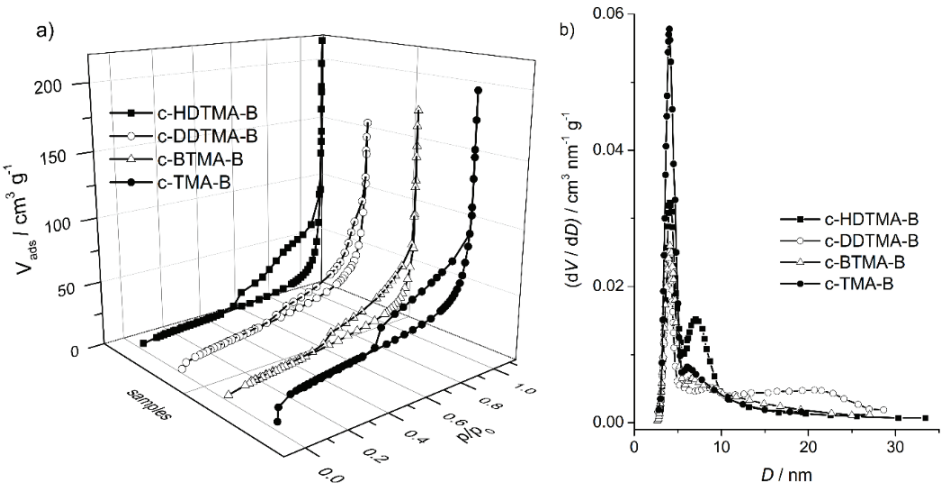

Fig. 2. a) Nitrogen adsorption/desorption isotherms recorded for carbonized bentonites; b) corresponding pore size distributions obtained by the Barrett–Joyner–Halenda (BJH) method.

All investigated samples were of Type IIb, according to the IUPAC classification, with the H3 type hysteresis loop.[21] The H3 loop is characteristic of powders and aggregates of plate-shaped particles, clays, and pigments. Hysteresis loops at higher relative pressures are the result of capillary condensation. Narrower hysteresis loops, such as those obtained for c-DDTMA-B and c-BTMA-B samples, usually indicate irregularly shaped aggregates.

The specific surface area and total pore volume (Table II) of the carbonized bentonites depended on the organic precursor used for the synthesis of organobentonites. The lowest value was obtained for c-HDTMA-B and the highest for

c-TMA-B reflecting the amount of carbon generated in the pores of bentonite upon the pyrolysis of the organic precursor.

TABLE II. Textural properties calculated from N_2 adsorption-desorption isotherms; S_{BET} is specific surface area; $V_{0.98}$ is total pore volume estimated from the amount of nitrogen adsorbed at the relative pressure of 0.98; D_{max} is the maximum pore diameter

Sample	S_{BET} / m^2 g^{-1}	$V_{0.98}$ / cm^3 g^{-1}	D_{max1} / nm	D_{max2} / nm	D_{max3} / nm
c-HDTMA-B	27	0.093	4.0	7.0	–
c-DDTMA-B	47	0.130	3.9	8.7	20.7
c-BTMA-B	34	0.102	4.1	6.7	–
c-TMA-B	89	0.127	4.0	6.1	–

The pore size distribution in the mesoporous region obtained by the BJH method (Fig. 2b) exhibits two peaks in the mesoporous region. The first peak had maxima at about 4.0 nm and is characteristic of clays rich in smectite.[32] The second peak had the maxima within the range from 6.1–8.7 nm and can be considered as the indicator of precursor influence. The third maximum at 20.7 appeared only for the c-DDTMA-B sample.

Raman spectroscopy

Raman spectra (Fig. 3) were recorded in the Raman shift range from 2200 to 800 cm^{-1}.

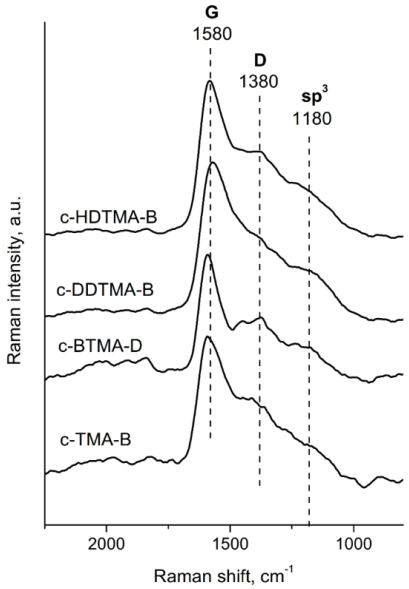

Fig. 3. Raman spectra of c-HDTMA-B, c-DDTMA-B, c-BTMA-B and c-TMA-B in the range between 2200 and 800 cm^{-1}.

The Raman spectra of the investigated carbonized clays were similar. The typical D and G bands can be observed at ~1580 and ~1380 cm^{-1} representing

the graphitized and disordered sp^2 structure. The G band corresponds to the in-plane, doubly degenerated E_{2g} phonon at the graphene Brillouin zone centre. The D peak is linked to the breathing modes of the sp^2 rings and requires a defect for its activation.[33] In addition, the band at 1180 cm^{-1} observed in all spectra could be attributed to the contribution of sp^3 carbon vibrations.[34] The appearance of the D peak is correlated to the presence of aromatic rings or the formation of clusters in the amorphous carbon.[35] The noticeable difference of the D peak in the c-HDTMA-B and c-DDTMA-B spectra are the result of different arrangements of the organic precursor in the smectite interlamellar space. HDTMA was arranged in a pseudo-trimolecular layer enabling the formation of more clusters. According to Ferrari and Robertson,[35] unlike in graphite, the development of the D peak in amorphous carbons indicates ordering. The same peak in the c-BTMA-B spectrum arose because of the presence of an aromatic ring.

Electrochemical properties of carbonized bentonite

The electrochemical properties of the carbonized bentonite were first tested using cyclic voltammetry in 1 mM potassium hexacyanoferrate (II) in 0.2 M KCl (Fig. 4a). All recorded cyclic voltammograms (CVs) showed the characteristic pair of peaks corresponding to the oxidation and the reduction of $[Fe(CN)_6]^{3-/4-}$. The response of anionic probe on cationic clay greatly depends on the modification of the clay. Smectite sheets have a permanent negative charge introduced by isomorphic substitution. It is expected that these charges would repel the anionic redox probe. However, the cationic sites present at the edges of clay particles[36] and/or introduced by clay modification provide the sites for interaction with the anionic probe. CVs recorded using c-HDTMA-B and c-DDTMA-B containing electrodes were similar, as expected, because of the similarity of molecules of the used organic precursors. The peak-to-peak separation was 0.43 V, I_a/I_c ratio was 1.05 and half-wave potential was 0.31 V. CV of c-BTMA-B electrode exhibited lower peak-to-peak separation of 0.23 V. The I_a/I_c ratio was 0.9 and the half-wave potential was 0.26 V. c-TMA-B electrode showed the highest current, although the peak corresponding to the oxidation of $[Fe(CN)_6]^{4-}$ was not well resolved. The estimated peak-to-peak separation and the half-wave potentials were 0.30 and 0.26 V, respectively. The shift of the half-wave potentials and peak-to-peak separation toward lower values for c-BTMA-B and c-TMA-B showed that $[Fe(CN)_6]^{4-}$ was more easily oxidized at these electrodes with faster electron transfer. The results of the CV of c-BTMA-B the I_a/I_c ratio to be below unity indicating better retention of the formed $[Fe(CN)_6]^{3-}$ at the electrode surface. The presence of $[Fe(CN)_6]^{3-}$ on the electrode surface additionally contributed to the repulsion, thus increasing the charge transfer resistance.

The response of the carbon paste electrode also depends on the source of carbon. In our previous publication,[37] we have investigated the influence of gra-

phite and carbon black on the response of carbon clay-based electrodes. Better results were obtained with carbon black, although the graphite-based electrodes showed improvement in comparison to the electrodes based only on carbon clay, without the addition of an external carbon source.

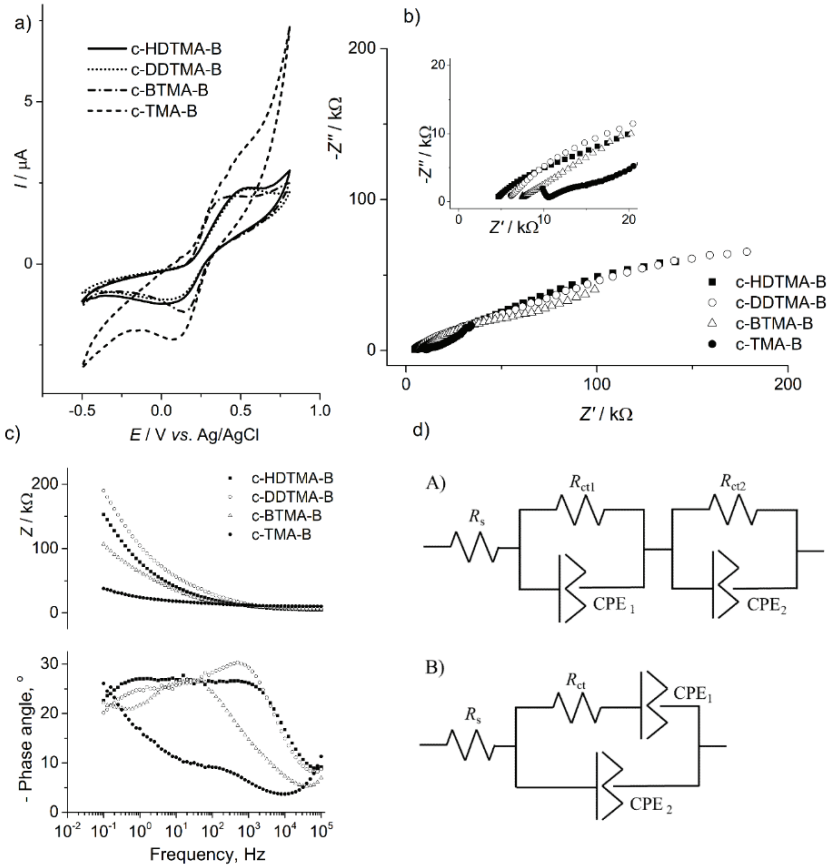

Fig. 4. Carbon paste electrodes modified with different clay samples: a) cyclic voltammograms recorded in 1 mM $K_4[Fe(CN)_6]$ + 0.2 M KCl at a scan rate of 50 mV s^{-1}; b) Nyquist plot recorded in the same solution in OCP; c) Bode plot recorded in the same solution in OCP; d) the equivalent electric circuit used to fit EIS data.

Further investigation was performed using the electrochemical impedance spectroscopy (EIS) in the same solution. The Nyquist plots obtained for the c--HDTMA-B and c-DDTMA-B electrodes (Fig. 4b) were similar to each other and consisted of two depressed semi-circles. The accompanying Bode plots (Fig. 4c) showed two relaxation time constants. Hence, these spectra were fitted with an equivalent circuit consisting of the series combination of an internal resistance R_s, a parallel R_{ct1}–CPE_1 and a parallel R_{ct2}–CPE_2 (equivalent circuit A). The

first R_{ct}–CPE pair corresponds to the charge transfer resistance and the capacitance accompanied with the charge transfer resistance. The second R_{ct}–CPE pair describes the second semi-circle at lower frequencies and corresponds to the ionic resistance in the electrode and the diffusion impedance. The Nyquist plots obtained for the c-BTMA-B electrode and the c-TMA-B electrode consisted of a semi-circle and the linear part. The accompanying Bode plots (Fig. 4c) exhibited one relaxation time constant. Hence, these spectra were fitted with a modified Randles circuit (equivalent circuit B) consisting of internal resistance (R_s) in a series with a parallel combination of a double-layer capacitance represented with a constant phase element (CPE_2) and an impedance of a faradaic reaction (serial combination of charge transfer resistance, R_{ct}, and a constant phase element (CPE_1)). The constant phase element (CPE) is often used to replace the double-layer capacitance (C_{dl}) and the Warburg impedance in the original Randles circuit. The capacitance element CPE will become the pure capacitance, pure resistance, and Warburg impedance when $n = 1$, $n = 0$ and $n = 0.5$, respectively. The resistor (R), capacitor (C) and Warburg impedance element (W) can, therefore, be considered to be a special case of CPE.[38] The results obtained using fitting with these circuits are presented in Table III. The highest value of charge transfer resistance was obtained for c-BTMA-B.

TABLE III. The electrochemical parameters obtained by fitting the EIS data recorded using the electrodes with the CB/clay ratio of 1:20 in 1 mM $K_4[Fe(CN)_6]$ in 0.2 M KCl

Electrode	R_s / kΩ	R_{ct1} / kΩ	Q_1[a] / μS s^{n_1}	n_1	R_{ct1} / kΩ	Q_2 /μS s^{n_2}	n_2
c-HDTMA-B	3.8	7.8	0.9	0.7	388	5.7	0.4
c-DDTMA-B	5.3	21.5	0.6	0.7	345	4.3	0.4
c-BTMA-B	7.0	105.0	25.7	0.6	4.1	–	0.5
c-TMA-B	9.8	12.5	29.3	0.5	9.1	–	0.4

[a]The impedance of constant phase element: $Z = 1/Y = 1/(i\omega)^n Q$; where Y is admittance, i is the imaginary unit, ω is the angular frequency, n is the exponent associated with the system inhomogeneity and Q has the numerical value of the admittance $1/|Z|$ at $\omega = 1$ rad/s

The behaviour of the redox probe $[Fe(CN)_6]^{3-/4-}$ is influenced by the electronic properties, microstructure, and surface properties of the electrode surface.[39] The investigated composites contained bentonite, and its negative surface charge repulses the negatively charged redox probe.[8] However, the positively charged pH-dependent sites enable the interaction of the clay-modified electrodes with the negatively charged redox probe.

At the pH of the used electrolyte (pH 5.5), >AlOH and >SiOH groups are present at the clay surface because of the deprotonation of $>AlOH_2^+$ and $>SiOH_2^+$ at lower pH values.[40] The PZC measurement[16] revealed that the contribution of a variable charge was less pronounced at carbonized clays, especially for those with higher carbon content. On the other hand, the carbonized bento-

nites showed to have a different distribution of surface groups in comparison with that of the starting bentonite. Besides that, they contain additional surface groups, such as >C=O, >COOH, >C-OH, $>NH_2$,[41,42] and some of them (>COOH groups) are shown to have an inhibitory effect on the electrochemistry of $Fe(CN)_6^{3-/4-}$.[43]

The intercept of the semicircle with the real axis at higher frequencies represents the internal resistance, R_S. The internal resistance mainly represents the resistance of the bulk electrolyte. The value of R_S increased in the following order: c-HDTMA-B < c-DDTMA-B < c-BTMA-B < c-TMA-B. The observed shift of the R_S to higher values can be ascribed to the increase of the ionic resistance of the electrode surface,[44] *i.e.*, the electrode layer adjacent to the bulk electrolyte. The increase of the thickness of this layer, *i.e.*, the increase of the depth of the electrolyte penetration into the electrode,[45] led to the increase of R_S.

The electrosorption properties of investigated carbonized bentonites were tested from 0.2 M NaCl and 0.2 M Na_2SO_4. The anodic polarization was applied to test the sorption of anions and the obtained chroncoulometric curves were normalized for the sake of comparison (Fig. 5).

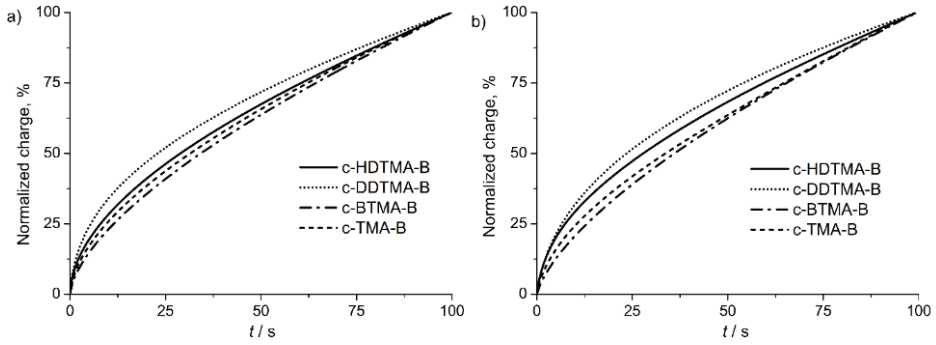

Fig. 5. Normalized chronocoulometric curves of carbonized bentonites in: a) 0.2 M NaCl and b) 0.2 M Na_2SO_4.

The time constant ($\tau = RC$) can be obtained by applying:[46]

$$-\ln\left(1-\frac{Q}{Q_0}\right)=\frac{t}{RC} \quad (1)$$

where Q_0 is the electrode's charge at the equilibrium, t is the time of the pulse, R is the resistance and C is the electrode's capacitance.

The time constant, obtained as a slope of the linear part of the plot, is presented in Table IV.

The electrosorption depends on the average pore dimensions,[47] the ionic charge and the hydrated radius.[48] The electrosorption was hindered by the pre-

sence of smaller pores resulting in the higher values of time constants. The values of the obtained time constants correlate with the values of the second maxima obtained from the N_2 adsorption-desorption isotherms: the higher the constant the smaller pore diameter. The shorter time constants were obtained for chlorides than for sulfates. The slower kinetics of electrosorption recorded for the sulfate ions is the consequence of their higher charge that caused stronger electrostatic interactions.

TABLE IV. Time constants (s) of the carbonized bentonite electrodes calculated from the chronocoulometric curves recorded in 0.2 M NaCl solution and 0.2 M Na_2SO_4 solution

Electrode	Solution	
	NaCl	Na_2SO_4
c-HDTMA-B	9.80	10.39
c-DDTMA-B	8.73	9.11
c-BTMA-B	10.29	11.33
c-TMA-B	10.75	11.40

CONCLUSION

Organomodified bentonite composite, prepared by the use of different alkylammonium salts (HDTMA, DDTMA, BTMA and TMA), was pyrolyzed and carbon-bentonite hybrid composites were obtained. The carbonized bentonites were characterized using the XRD, low-temperature N_2 physisorption and Raman spectroscopy. The structure with the defined d_{001} basal spacing was found only for HDTMA-derived sample, while the samples derived from organoclays with shorter chains showed the presence of collapsed structures. Extreme values of the specific surface area and pore volume were obtained for the carbonized clay originating from the bentonite modified with the surfactant with the highest and lowest numbers of carbon atoms. The Raman spectroscopy confirmed the formation of amorphous carbon in the carbonized bentonites.

Electrochemical impedance spectroscopy and cyclic voltammetry showed that the carbonized bentonite sample derived from TMA-clay exhibited the highest electrochemical activity toward the $Fe(CN)_6^{3-/4-}$ redox couple. The internal resistance of the samples increased with the decrease of the chain length of the used organic precursor. The chronocoulometry was used to study the electrosorption properties of carbonized bentonites toward chloride and sulphate ions. The electrosorption was hindered at the samples with smaller pores. The type of organic precursor influenced the pore size of the carbonized bentonite and their electrosorption properties.

Acknowledgment. This work was financially supported by the Ministry of Education, Science and Technological Development of the Republic of Serbia (Grant No. 451-03-9/2021--14/200026).

ИЗВОД

ЕЛЕКТРОХЕМИЈСКА СВОЈСТВА КАРБОНИЗОВАНИХ БЕНТОНИТА

НАТАША П. ЈОВИЋ-ЈОВИЧИЋ[1], ДАНИЦА В. БАЈУК БОГДАНОВИЋ[2], ТАТЈАНА Б. НОВАКОВИЋ[1], ПРЕДРАГ Т. БАНКОВИЋ[1], АЛЕКСАНДРА Д. МИЛУТИНОВИЋ-НИКОЛИЋ[1] и ЗОРИЦА Д. МОЈОВИЋ[1]

[1]Универзитет у Београду - Институт за хемију, технологију и металургију, Центар за катализу и хемијско инжењерство, Његошева 12, 11 000 Београд и [2]Факултет за физичку хемију, Универзитет у Београду, Студентски трг 12–16, 11 000 Београд

Органомодификовани бентонити су добијени модификацијом бентонита из локалног рудника Боговина са четири различита алкиламонијум јона у количини која је једнака његовом капацитету јонске измене. Карбонизовани бентонити, добијени пиролизом органомодификованих бентонита у струји азота, окарактерисани су помоћу дифракције X-зрачења (XRD), нискотемпературском физисорпцијом азота и Раманском спектроскопијом. Структурна и текстурална својства карбонизованих бентонита зависе од уређења алкиламонијум катјона у одговарајућем полазном органомодификованом бентониту. Резултати карактеризације су показали да особине узорака зависе од распореда алкиламонијум катјона у органомодификованом бентониту од ког су настали, док је Раманска спектроскопија потврдила присуство аморфног угљеника. Добијени карбонизовани бентонити су коришћени за модификацију електроде од пасте угљеника. Модификоване електроде су испитане помоћу цикличне волтаметрије и електрохемијске импедансне спектроскопије. Електросорпција хлорида и сулфата је проучавана помоћу хронокулонометрије. Резултати су протумачени на основу присутних површинских група и текстуралних својстава карбонизованих бентонита.

(Примљено 27. јануара, ревидирано 22. марта, прихваћено 26. марта 2022)

REFERENCES

1. M. F. Brigatti, E. Galán, B. K. G. Theng, in *Handbook of Clay Science, Developments in Clay Science*, F. Bergaya, G. Lagaly (Eds.), Elsevier, Amsterdam, 2013, pp. 21–81 (ISBN: 978-0-08-098259-5)
2. P.K. Ghosh, A.J. Bard, *J. Am. Chem. Soc.* **105** (1983) 5691 (https://doi.org/10.1021/ja00355a030)
3. S. M. Macha, A. Fitch, *Microchim. Acta* **128** (1998) 1 (https://doi.org/10.1007/BF01242184)
4. Z. Navratilova, P. Kula, *Electroanalysis* **15** (2003) 837 (https://doi.org/10.1002/elan.200390103)
5. I. K. Tonle, E. Ngameni, A. Walcarius, *Sensors Actuators, B* **110** (2005) 195 (https://doi.org/10.1016/j.snb.2005.01.027)
6. P. Falaras, F. Lezou, *J. Electroanal. Chem.* **455** (1998) 169 (https://doi.org/10.1016/S0022-0728(00)00133-9)
7. D. Petridis, P. De S. Kaviratna, T.J. Pinnavaia, *J. Electroanal. Chem.* **410** (1996) 93 (https://doi.org/10.1016/0022-0728(96)04541-X)
8. I. K. Tonle, E. Ngameni, F. M. M. Tchieno, A. Walcarius, *J. Solid State Electrochem.* **19** (2015) 1949 (https://doi.org/10.1007/s10008-014-2728-0)
9. P. R. Vernekar, N. P. Shetti, M. M. Shnbhag, S. J. Malode, R .S. Malladi, K. R. Reddy. *Microchim. J.* **159** (2020) 105441 (https://doi.org/10.1016/j.microc.2020.105441)

10. N. P. Shetti, S. J. Malode, D. S. Nayak, R. R. Naik, G. T. Kuchinad, K. R. Reddy, S. S. Shukla, T. M. Aminabhavi, *Michochim. J.* **155** (2020) 104727 (https://doi.org/10.1016/j.microc.2020.104727)
11. N. P. Shetti, D. S. Nayak, S. J. Malode, *Vacuum* **155** (2018) 524 (https://doi.org/10.1016/j.vacuum.2018.06.050)
12. P. Aranda, M. Darder, R. Fernández-Saavedra, M. Lopez-Blanco, E. Ruiz-Hitzky, *Thin Solid Films* **495** (2006) 104 (https://doi.org/10.1016/j.tsf.2005.08.284)
13. M. Darder, E. Ruiz-Hitzky, *J. Mater. Chem.* **15** (2005) 3913 (https://doi.org/10.1039/B505958E)
14. A. Gómez-Avilés, M. Darder, P. Aranda, E. Ruiz-Hitzky, *Angew. Chem. Int. Ed. Engl.* **46** (2007) 923 (https://doi.org/10.1002/anie.200603802)
15. C. Zhang, D. He, J. Ma, W. Tang, T. D. Waite, *Water Res.* **128** (2018) 314 (https://doi.org/10.1016/j.watres.2017.10.024)
16. N. Jović-Jovičić, M. Mojović, D. Stanković, B. Nedić-Vasiljević, A. Milutinović-Nikolić, P. Banković, Z. Mojović, *Electrochim. Acta* **296** (2019) 387 (https://doi.org/10.1016/j.electacta.2018.11.031)
17. S. Biniak, A. Swiatkowski, M. Pakuła, M. Sankowska, K. Kuśmierek, G. Trykowski, *Carbon* **51** (2013) (https://doi.org/10.1016/j.carbon.2012.08.057)
18. P. Baskaralingam, M. Pulikesi, D. Elango, V. Ramamurthi, S. Sivanesan, *J. Hazard. Mater.* **128** (2006) 138 (https://doi.org/10.1016/j.jhazmat.2005.07.049)
19. EPA, *Method 9080: Cation-exchange capacity of soils (ammonium acetate)*, https://www.epa.gov/sites/production/files/2015-12/documents/9080.pdf
20. N. Jović-Jovičić, A. Milutinović-Nikolić, M. Žunić, Z. Mojović, P. Banković, I. Gržetić, D. Jovanović, *J. Contam. Hydrol.* **150** (2013) 1 (https://doi.org/10.1016/j.jconhyd.2013.03.004)
21. F. Rouquerol, J. Rouquerol, K. S. W. Sing, P. Llewellyn, G. Maurin, *Adsorption by powders and porous solids, principles, methodology and applications*, Academic Press, New York, 2012 (https://doi.org/10.1016/B978-0-12-598920-6.X5000-3)
22. B. C. Lippens, B. G. Linsen, J. H. De Boer, *J. Catal.* **3** (1964) 32 (https://doi.org/10.1016/0021-9517(64)90089-2)
23. K. S. Sing, *Pure Appl. Chem.* **57** (1985) 603 (https://doi.org/10.1351/pac198557040603)
24. International Center for Diffraction Data, Joint Committee on Powder Diffraction Standards (JCPDS), Swarthmore, PA, 1990
25. N. Jović-Jovičić, A. Milutinović-Nikolić, P. Banković, B. Dojčinović, B. Nedić, I. Gržetić, D. Jovanović, *Acta Phys. Pol., A* **117** (2010) 849 (https://doi.org/10.12693/APhysPolA.117.849)
26. A. Abu Rabi-Stanković, A. Milutinović-Nikolić, N. Jović-Jovičić, P. Banković, M. Žunić, Z. Mojović, D. Jovanović, *Clays Clay Miner.* **60** (2012) 291 (https://doi.org/10.1346/CCMN.2012.0600306)
27. A. Abu Rabi-Stanković, Z. Mojović, A. Milutinović-Nikolić, N. Jović-Jovičić, P. Banković, M. Žunić, D. Jovanović, *Appl. Clay Sci.* **77**–**78** (2013) 61 (https://doi.org/10.1016/j.clay.2013.04.003)
28. P. Banković, A. Milutinovic-Nikolic, Z. Mojović, N. Jović-Jovičić, M. Perovic, V. Spasojevic, D. Jovanović, *Micropor. Mesopor. Mater.* **165** (2013) 247 (https://doi.org/10.1016/j.micromeso.2012.08.029)

29. C. Ruiz-García, J. Perez-Carvajal, A. Berenguer-Murci, M. Darder, P. Aranda, D. Cazorla-Amoros, E. Ruiz-Hitzky, *Phys. Chem. Chem. Phys.* **15** (2013) 18635 (https://doi.org/10.1039/C3CP53258E)
30. P Anadão, E. A. Hildebrando, I. L. R. Pajolli, K. R. de Oliveira Pereira, H. Wiebeck, F. R. V. Díaz, *Appl. Clay Sci.* **53** (2011) 288 (https://doi.otg/10.1016/j.clay.2011.04.022)
31. Q. Chen, R. Zhu, W. Deng, Y Xu, J. Zhu, Q. Tao, H. Hongping, *Appl. Clay Sci.* **100** (2014) 112 (https://doi.org/10.1016/j.clay.2014.04.011)
32. U. Kuila, M. Prasad, *Geophys. Prospect.* **61** (2013) 341 (https://doi.org/10.1111/1365-2478.12028)
33. O. Frank, G. Tsoukleri, I. Riaz, K. Papagelis, J. Parthenios, A. C. Ferrari, A. K. Geim, K.S. Novoselov, C. Galiotis, *Nat. Commun.* **2** (2011) 255 (https://doi.org/10.1038/ncomms1247)
34. J. Schwan, S. Ulrich, V. Batori, H. Ehrhardt, S. R. P. Silva, *J. Appl. Phys.* **80** (1996) 440 (https://doi.org/10.1063/1.362745)
35. A. C. Ferrari, J. Robertson, *Phys. Rev., B* **61** (2000) 14095 (https://doi.org/10.1103/PhysRevB.61.14095)
36. A. Fitch, *Clays Clay Miner.* **38** (1990) 391 (https://doi.org/10.1346/CCMN.1990.0380408)
37. C. Apetrei, I. M. Apetrei, J. A. De Saja, M. L. Rodriguez-Mendez, *Sensors* **11** (2011) 1328 (https://doi.org/10.3390/s110201328)
38. B.T. Mark, E. Orazem, *Electrochemical Impedance Spectroscopy*, John Wiley & Sons, Inc, Hoboken, NJ, 2008 (https://doi.org/10.1002/9780470381588)
39. R. L. McCreery, *Chem. Rev.* **108** (2008) 2646 (https://doi.org/10.1021/cr068076m)
40. A. Kriaa, N. Hamdi, E. Srasra, *Russ. J. Electrochem.* **43** (2007) 167 (https://doi.org/10.1134/S102319350702005X)
41. S. Gu, X. Kang, L. Wang, E. Lichtfouse, C. Wang, *Environ. Chem. Lett.* **17** (2019) 629 (https://doi.org/10.1007/s10311-018-0813-9)
42. L. Zhang, J. Cao, *J. Therm. Anal. Calorim.* **137** (2019) 1 (https://doi.org/10.1007/s10973-018-7947-7)
43. M. M. Lounasvuori, M. Rosillo-Lopez, C. G. Salzmann, D. J. Caruana, K. B. Holt, *Faraday Discuss.* **172** (2014) 293 (https://doi.org/10.1039/C4FD00034J)
44. H. Nara, D. Mukoyama, R. Shimizu, T. Mommaa, T. Osaka, *J. Power Sources* **409** (2019) 139 (https://doi.org/10.1016/j.jpowsour.2018.09.01)
45. Y. Abe, N. Hori, S. Kumagai, *Energies* **12** (2019) 4507 (https://doi.org/10.3390/en12234507)
46. M. Noked, E. Avraham, A. Soffer, D. Aurbach, *J. Phys. Chem., C* **113** (2009) 21319 (https://doi.org/10.1021/jp905987j)
47. G. Rasines, P. Lavel, C. Macías, M. Haro, C. O. Ania, J. L. Tirado, *J. Electroanal. Chem.* **671** (2012) 92 (http://dx.doi.org/10.1016/j.jelechem.2012.02.025)
48. Z. Chen, H. Zhang, C. Wu, Y. Wang, W. Li, *Desalination* **369** (2015) 46 (https://doi.org/10.1016/j.desal.2015.04.022).